

1
2
3 Enhanced SO₂ adsorption and desorption on
4 chemically and physically activated biochar
5 made from wood residues

6
7
8 Flavia Lega Braghiroli ^{*1,2}, Hassine Bouafif ², Ahmed Koubaa ¹

9
10 ¹ Research Forest Institute (Institut de recherche sur les forêts - IRF), University of Québec in
11 Abitibi-Témiscamingue (UQAT), 445 Boul. de l'Université, Rouyn-Noranda, QC J9X 5E4,
12 Canada

13 ² Centre Technologique des Résidus Industriels (CTRI, Technology Center for Industrial Waste),
14 Cégep de l'Abitibi-Témiscamingue (College of Abitibi-Témiscamingue), 425 Boul. du Collège,
15 Rouyn-Noranda, QC J9X 5E5, Canada

16
17 * Corresponding author: (F.L. Braghiroli)

18 Tel: +1 (819)-762-0931 ext. 1748;

19 Fax: +1 (819)-762-0906;

20 Email: Flavia.Braghiroli@uqat.ca

21 **Abstract**

22 SO₂, one of the most harmful gases, is generated when oxygen in air combines with sulfur species
23 from anthropogenic sources (e.g., the smelting of mineral ores). Thus, the objectives of this study
24 are to assess the potential use of activated biochar for the removal of SO₂, and to compare the
25 impact of the activation process on the development of porosity and surface chemistry for SO₂
26 adsorption. Results show that activated biochars develop porosity (with narrow and wide pores)
27 and functional groups connected to their surface, which makes these materials suitable for
28 adsorption of SO₂. However, no linear relationship between textural properties and the amount of
29 SO₂ adsorbed by activated biochars **from dynamic adsorption tests** were noticed. In addition, the
30 highest SO₂ adsorption capacity was not reached for materials with the highest surface area, or
31 micropore or ultramicropore volume. Specifically, steam-activated biochar had the best
32 performance for the removal of SO₂ due to its optimal surface area (590 m² g⁻¹); volume of ultra-
33 (0.22 cm³ g⁻¹), micro- (0.23 cm³ g⁻¹), and mesopores (0.11 cm³ g⁻¹); its basic character (not from
34 nitrogenated groups); and the low percentage of acid-oxygenated functional groups connected to
35 its surface. After six thermal regeneration cycles, activated biochar exhibited high SO₂ removal
36 capacity and high regenerability. Based on these findings, activated biochar made from forest wood
37 residues has promising potential for the removal of gas contaminants.

38 **Keywords:** Activated biochar, SO₂ removal, adsorption, porosity, surface chemistry

39

40

41

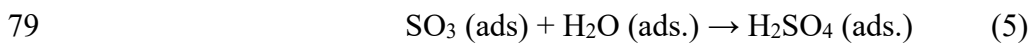
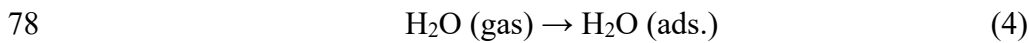
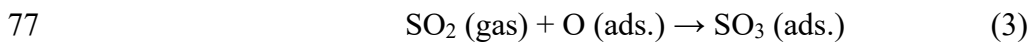
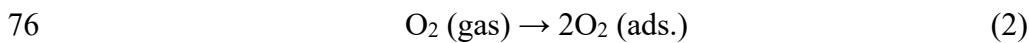
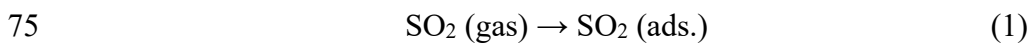
42

43 **1. Introduction**

44 Researchers have been working to develop efficient technologies that will reduce toxic
45 pollutants in the air. A colorless gas with a strong odor, SO₂ is produced when oxygen in air
46 combines with sulfur gas emissions. It is one of the world's major air pollutants and can also easily
47 react with other substances to form harmful components (e.g., sulfuric acid, sulfurous acid, and
48 sulfate particles) (He et al., 2003). The majority of this gas in air comes from human sources, apart
49 from the natural emissions from volcanoes. SO₂ is the major air pollutant produced by industrial
50 activities, especially from the burning of fossil fuels (coal, oil, and gas) for the generation of
51 electricity or the smelting of mineral ores (i.e., aluminum, copper, zinc, lead, and iron) that contain
52 sulfur (Fioletov et al., 2016). The SO₂ generated by industry contributes to urban air pollution that
53 affects human health and well-being and life expectancy (Khaniabadi et al., 2017). Several
54 international agreements aim to reduce emissions of air pollutants. For instance, the Canada–United
55 States Air Quality Agreement of 1991 aims to reduce the impact of transboundary air pollution
56 (Environment and Climate Change Canada, 2018), whereas the 1994 Oslo Protocol on Further
57 Reduction of Sulfur Emissions, signed by Canada and several European countries, intends not only
58 to take effective measures for the reduction of sulfur but also to use renewable energy and efficient
59 technologies to deal with air pollution (UNECE, 2018).

60 The techniques used in industry for SO₂ removal are based on the principle of gas–liquid
61 reactions, using liquid alkaline solutions (e.g., Mg(OH)₂, Ca(OH)₂) (Slack et al., 1972; Li and Zhu,
62 2016), or solid–gas reactions, using carbon-derived materials (e.g., activated carbon) (Shafeeyan et
63 al., 2010; Abdurashed et al., 2018; Bamdad et al., 2018). The first procedure generates
64 considerable by-products, whereas the adsorption of SO₂ over carbon materials has been the most
65 viable and effective alternative because of the ease of installation and operation of gas adsorption

66 apparatus, as well as simple carbon's regeneration. Indeed, activated carbon is the most widely used
67 material for the removal of gaseous pollutants at various concentrations (Mohamad Nor et al.,
68 2013). However, a SO₂ removal mechanism is not well established due to the complexity of the
69 surface porous structure of activated carbons made from abundant low-cost biomass residue
70 precursors. It is known that during the process of SO₂ adsorption in O₂ atmosphere and in presence
71 of H₂O in the gas phase, several reactions may be performed (Eqs. 1–5). These elements will be
72 first adsorbed (ads.) onto the carbon material (Eq. 1–3), and then oxidation of SO₂ to SO₃ (Eq. 4)
73 and the formation of H₂SO₄ (Eq. 5) on the surface of carbon material will be accomplished
74 (Lisovskii et al., 1997; Bagreev et al., 2002):



80 The surface chemistry of activated carbons plays a major role on their performance for SO₂
81 adsorption. It was reported that basic and acid groups connected to the surface of carbon material
82 can improve SO₂ uptake. For some researchers, the presence of basic groups strengthens the bond
83 of H₂SO₄ to the materials' surface (Raymundo-Piñero et al., 2000; Davini, 2001; Bagreev et al.,
84 2002), whereas for others, acid groups weaken the adsorption energy for H₂SO₄, improving the
85 extractability of H₂SO₄ by water (Lisovskii et al., 1997) and, consequently, enhancing SO₂
86 adsorption. The porous structure of the activated carbon can also have an effect on the SO₂
87 adsorption, but this process is still controversial. Karatepe et al. (2008) stated that the porous
88 structure, rather than specific surface area, of chemically and physically activated carbons

89 contributed to SO₂ adsorption. They also reported a linear relationship between the micropore
90 volume and the amount of SO₂ adsorbed. For Zhu et al. (2012), the highest SO₂ adsorption capacity
91 does not exist at the largest micropore volume, while a linear relationship was found between the
92 ultramicropore volume of CO₂-activated carbons and SO₂ adsorbed. For Raymundo-Piñero et al.
93 (2000), SO₂ adsorption capacity is related to narrow micropore volume; thus, oxidation of SO₂ to
94 SO₃ (Eq. 3) occurs in pores lower than 0.7 nm independent of the nature and surface chemistry of
95 the material.

96 Other materials such as biochar, a by-product carbon-rich material produced from the
97 thermochemical conversion (i.e., torrefaction, slow to fast pyrolysis, and gasification) of biomass
98 waste materials (Rangabhashiyam and Balasubramanian, 2019), have been recently studied for SO₂
99 removal. According to Xu et al. (2016), biochars made from dairy manure, sewage sludge, and rice
100 husk presented SO₂ sorption capacities of up to 64 mg g⁻¹. Materials had a basic character but low
101 specific surface area (up to 42 m² g⁻¹); thus, SO₂ sorbed was due to mineral components in biochar
102 that could react with SO₂ to form various sulfate minerals on its surface. This result could be also
103 improved with the activation of biochars, but few studies reported its use for SO₂ removal. Shao et
104 al. (2018) has recently shown that CO₂ activation of corncobs biochar improved its porosity (755
105 m² g⁻¹) and SO₂ adsorption capacity to up to 58 mg g⁻¹. In addition, amine impregnation onto
106 activated biochar has found to develop a surface chemistry basicity, with an increase of nitrogen
107 content, that has a strong interaction with SO₂ contaminant (Shao et al., 2018).

108 Thus, the objectives of the present study are investigating the role of the porous structure and
109 surface chemistry of activated biochars made from wood residues and pilot-scale technologies of
110 fast pyrolysis and activation on their performance for SO₂ adsorption capacity and thermal
111 regeneration.

112 2. Materials and methods

113 2.1 Synthesis of activated biochar

114 In this study, black spruce (BS) and white birch (WB) residues were sampled from sawmills
115 and converted into biochars (BBS and BWB) by fast pyrolysis at 454 °C through CarbonFX fast
116 pyrolysis technology (Airex Energy, Bécancour, QC, Canada). Biochars were then milled at 1–2
117 mm (Grinder: Ro-tap RS-29, WS Tyler, Mentor, OH, USA) and activated in a homemade pilot
118 oven in presence of three types of activating agents: KOH, CO₂, and superheated steam. In chemical
119 activation, 100 g of biochar was mixed with 200 g of water and 100 g KOH pellets. The mixture
120 was left in the fume hood for 2 h and then, continue drying in an oven at 120°C overnight. Then,
121 the impregnated material was activated at 900 °C for approximately 67 min in N₂ atmosphere. The
122 same procedure was carried out in physical activation, in which the flowing gas of CO₂ (3 L min⁻¹)
123 or steam (0.3 L min⁻¹) was introduced when the temperature reached 900 °C for approximately 67
124 min. The activated biochars were labeled KOHBWB, KOHBBS, CO₂BWB, CO₂BBS, H₂O BWB
125 and H₂O BBS, depending on the type of activation agent and wood residue.

126 2.2 Physicochemical characterization

127 The prepared biochars and activated biochars were characterized by pH, elemental composition
128 (C, H, N, S, O), surface chemistry, specific surface area and pore volume. The pH of the resultant
129 filtrate, obtained by mixing 0.4 g of biochar-derived material with 20 mL of distilled water
130 overnight, before (pH_i), and after (pH_f) SO₂ adsorption, was measured using a SevenMulti, Mettler
131 Toledo (Greifensee, Switzerland) equipped with Inlab Routine Pro electrode. Perkin Elmer 2400
132 CHNS/O Analyzer (Waltham, MA, USA) was used for the determination of C, H, N, S, O elements,
133 whereas Kratos AXIS ULTRA X-ray photoelectron spectroscopy (XPS) (Wharfside, MA, UK) was
134 used for analyzing the surface chemistry of the prepared materials.

135 The pore texture parameters of biochars and activated biochars were obtained by CO₂
136 adsorption at 0 °C and N₂ adsorption at -196 °C, respectively, using a Micromeritics ASAP 2460
137 automatic apparatus (Norcross, GA, USA). After treatment of N₂ adsorption-desorption isotherms,
138 the most important parameters were obtained: i) surface area: S_{BET} (m² g⁻¹) (Brunauer et al., 1938);
139 ii) micropore volume: V_{μN₂} (cm³ g⁻¹) (Dubinin, 1989); iii) total pore volume: V_t (cm³ g⁻¹) (Gregg
140 and Sing, 1991); iv) mesopore volume: V_m (cm³ g⁻¹); and v) average pore width calculated by the
141 Stoeckli-Ballerini equation (Stoeckli and Ballerini, 1991). Ultramicroporosity (V_{μCO₂}) and pore size
142 distribution (PSD) (Tarazona, 1995) were obtained through CO₂ and N₂ adsorption isotherms,
143 respectively.

144 2.3 SO₂ adsorption and materials' regeneration tests

145 Dynamic tests were carried out at room temperature (~ 20 °C) to evaluate the capacity of
146 biochars and activated biochars for SO₂ adsorption. The apparatus and conditions used for
147 determining SO₂ breakthrough capacity were chosen according to the standard test method: *ASTM*
148 *D6646-03 (2008)* (ASTM Standard D6646-03, 2008). Materials were placed into a glass column
149 (27 cm length, 2.5 cm diameter) at different weighs (10–25 g) due to their various densities. Then,
150 50 ppm of SO₂ with moist air passed through the column at 30 mL min⁻¹. The outlet concentration
151 of SO₂ was measured using a GazBadger®Pro flue gas meter (Industrial Scientific, Pittsburgh,
152 USA), and the test was stopped when the outlet concentration equaled the inlet concentration. The
153 SO₂ efficiency removal was calculated by Eq. 6:

$$154 \quad \text{SO}_2 \text{ removal efficiency} = \frac{C_{0 \text{ SO}_2} - C_{\text{SO}_2}}{C_{0 \text{ SO}_2}} \cdot 100\% \quad (6)$$

155 where C_{0 SO₂} and C_{SO₂} were the inlet and outlet SO₂ concentration, respectively, measured by the
156 flue gas meter. SO₂ saturation capacities were calculated by integrating the area above the saturation
157 curves and saturation time. The saturation tests were repeated at least five times to make sure that

158 the textural properties and consequently, the SO₂ adsorption capacities of activated biochars
159 prepared in a prototype pilot activation furnace were reproducible. During the regeneration cycle,
160 the saturated material was placed in the activation furnace at 600 °C for 1 h in N₂ atmosphere. The
161 adsorption–desorption cycle was repeated six times, and the SO₂ adsorption capacity (mg g⁻¹) after
162 each regeneration cycle was then calculated.

163 3. Results and discussion

164 3.1 SO₂ adsorption

165 Significant differences in the performance of biochars and activated biochars can be seen in
166 SO₂ breakthrough curves (Fig. 1) and the calculated SO₂ capacities (Table 1). H2OBWB obtained
167 the highest adsorption capacity of 76.9 mg g⁻¹, followed by CO2BWB (56.9 mg g⁻¹), KOHBWB
168 (35.3 mg g⁻¹), CO2BBS ~ KOHBBS ~ H2OBBS (~ 25.0–26.5 mg g⁻¹), and finally both biochars (~
169 20.4 mg g⁻¹). Activated biochars had a basic character (pH of between 8.2 and 10.3); after SO₂
170 adsorption, however, their pH was reduced to between 2.1 and 3.3, whereas biochars had an acid-
171 neutral and acid character before (pH 5.9–7.1) and after (pH 4.1–4.4) SO₂ adsorption, respectively.
172 This physical characteristic may explain the formation of H₂SO₄ (Eqs. 1–5) during SO₂ adsorption.
173 It implies that SO₂, O₂, and H₂O were adsorbed on the internal surface of biochar-derived materials
174 close enough and in appropriate steric configuration to react and form H₂SO₄ that was then
175 transported to accessible inner pores (Izquierdo et al., 2003).

176 To explain the differences in SO₂ adsorption capacity of activated biochars, both porosity and
177 surface chemistry were considered. First, analysis of the textural properties of biochars shows that
178 they are highly ultramicroporous, with surface areas of 177 and 208 m² g⁻¹ for BWB and BBS,
179 respectively. The modification of biochar structure is an alternative for improving the pore
180 structure, surface area, and its surface chemistry, determinant characteristics for enhancing SO₂

181 adsorption over carbon materials. Thus, after activation, birch-activated biochars presented highly
182 developed porosity with surface areas in the presence of KOH, CO₂, and steam of 1700, 881, and
183 590 m² g⁻¹, respectively, while spruce materials had slightly lower surface areas of 1662, 735, and
184 412 m² g⁻¹, respectively. Indeed, activation of biochars in the presence of CO₂ or superheated steam
185 agents promoted the removal of carbon atoms that generated a porous structure (Marsh and
186 Rodríguez-Reinoso, 2006; Giudicianni et al., 2017; Gargiulo et al., 2018). In the case of chemical
187 activation in the presence of KOH, the mechanism is more complex due to the presence of several
188 reactions that contribute to pore development. First, the reaction of carbon with KOH produces
189 K₂CO₃, H₂, and K, which enlarges material's pore size through intercalation with carbon sheets.
190 Then, carbon is consumed by K₂CO₃ to produce CO; at higher temperatures (> 800°C), K₂CO₃ is
191 decomposed into CO₂ and K₂O, which are further broken down into K and CO (Dehkhoda et al.,
192 2016). The resultant gases also contribute as physical agents during chemical activation, and, for
193 this reason, the highest porosity development was found in KOH-activated biochars.

194 N₂ adsorption–desorption isotherms of birch- and spruce-activated biochars are presented in
195 Figs. 2 a) and b), respectively. KOH-activated biochars and H2OBBS had an isotherm of Type I,
196 according to IUPAC classification (Sing, 1985), typical of microporous materials presenting an
197 elbow at P/P₀ at 0.05 followed by a horizontal plateau. Whereas a combination of isotherms Type
198 I and IV is typical of the existence of narrow microporosity and mesoporosity with the presence of
199 a narrow hysteresis loop for CO₂-activated biochars and H2OBWB (Braghiroli et al., 2018). PSDs
200 obtained by application of density functional theory (DFT) (Fig. 2 c) and d)) were in good
201 agreement with results obtained from N₂ isotherms. Activated birch biochars presented the highest
202 proportion of CO₂ adsorbed in ultramicropores compared to spruce materials (Figs. 2 e) and f)),
203 while KOH activation produced the highest proportion of ultramicropores, followed by CO₂ and

204 steam. Figs. 2 g) and h) show the PSD calculated by application of the DFT model to CO₂ isotherms.
205 The DFT curves of birch-activated biochars and H2OBBS show pores between 0.4 and 0.8 nm and
206 from 0.8 to > 1 nm, while CO2BBS and H2OBBS showed three peaks; one from 0.4 to 0.7 nm,
207 another between 0.7 and 0.8 nm, and the last between 0.8 and 0.9 nm.

208 The surface area of carbon materials is often related to their adsorption capacity. For Atanes et
209 al. (2012), the highest SO₂ uptake on cork-powder-activated carbon was consistent with its large
210 surface area; but the adsorption behavior for CO₂-lignite-activated carbon, which had the highest
211 surface area, did not follow this trend (Karatepe et al., 2008). The plots of the amount of SO₂
212 adsorbed from dynamic tests versus the surface area, different pore volumes (micropore, mesopore
213 and ultramicropore volume) and the average pore width of activated biochars (Fig. 3 a), b), c), d)
214 and e)) reveal that there is no linear relationship between them. The dependence between SO₂
215 sorbed and textural properties is usually obtained at equilibrium test conditions. Therefore, in this
216 study, it might have some kinetic limitations during SO₂ adsorption at dynamic test conditions. In
217 addition, similar to Karatepe et al. (2008), the highest surface area obtained for KOH-activated
218 biochars does not mean that they presented the highest SO₂ adsorption. Notably, rather optimal
219 textural properties – e.g., S_{BET}, V_t, average pore width, V_{μ N2} and V_{μ CO2} of 590 m² g⁻¹, 0.34 cm³ g⁻¹,
220 1, 0.80 nm, 0.23 cm³ g⁻¹, and 0.22 cm³ g⁻¹, respectively – are associated with H2OBWB and SO₂
221 sorbed.

222 Micropore volume in carbon materials was found to be the most important parameter to affect
223 gas pollutant adsorption (Lua and Guo, 2000). However, the material with the highest micropore
224 or ultramicropore volumes (Fig. 3 b) and d), respectively) did not adsorb the highest proportion of
225 SO₂. The relationship between mesopore volume (Fig. 3 c) and SO₂ uptake is not obvious, even
226 though materials with 0 % of mesopores, such as KOHBWB and KOHBBS, had the lowest SO₂

227 adsorption capacity. Raymundo-Pinero et al. (2000) noticed a linear relationship between
228 ultramicropore volume and adsorbed SO₂, even though activated carbons with a ultramicropore
229 volume higher than 0.4 cm³ g⁻¹ deviated from the trend. In this work, SO₂ adsorption was
230 diminished for materials having ultramicropore volume in the range of 0.20 cm³ g⁻¹ as well as at
231 higher than 0.30 cm³ g⁻¹. In the first case, similar to Karatepe et al.'s (2008) findings, the narrow
232 micropores, which comprised between 0.14 and 0.18 cm³ g⁻¹, were unfavorable to SO₂ adsorption
233 because materials could have different pore geometries that restricted the diffusion of SO₂
234 molecules. In the second case, similar to Raymundo-Piñero et al.'s (2000) findings, materials with
235 a wide microporosity showed less SO₂ adsorption simply because the ability for oxidation of SO₂
236 into SO₃ inside the micropores did not take place.

237 The SO₂ adsorption behavior for the most porous activated biochars (i.e., KOHBWB and
238 KOHBBS) do not follow the general trend. Their performance for SO₂ uptake was not consistent
239 with their textural properties, but it could be related with surface functional groups that might be
240 responsible for inhibiting SO₂ adsorption. Therefore, oxygenated functional groups connected to
241 the surface of biochar-derived materials were examined by XPS analysis. The primary C1s peak
242 was divided into five peaks at different binding energies of < 285eV, 285.7 < BE < 287.1, 286.1 <
243 BE < 288, 288 < BE < 289.4 and BE > 290 corresponding to C–C, C–OH, C=O or O–C–O, O=C–
244 O and $\pi \rightarrow \pi^*$, respectively. The peak area percentage shown in [Table 1](#) indicates the content of
245 each functional group. Activated biochars presented the highest percentage of graphitic sp² carbon
246 followed by C–OH, C=O or O–C–O and O=C–O groups. KOH-activated biochars presented the
247 highest proportion of these oxygenated groups (25.4 %) followed by CO₂ and steam-derived
248 materials (13.4 % for H2OBBS).

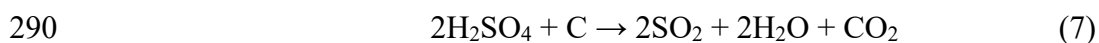
249 The comparison of SO₂ uptake and the total oxygenated groups (%) measured by XPS analysis
250 and the nitrogen content (%) from elemental analysis (already reported in (Braghiroli et al., 2018))
251 are given in Fig. 4 a) and b), respectively. The material that showed the highest proportion of SO₂
252 sorbed (H2OBWB) had one of the lowest percentage of acid-oxygenated groups (17.9 %), i.e.,
253 phenolic, lactonic, and carboxylic acid. Although an important amount of acid groups appeared on
254 the surface of activated biochars, the measured pH indicated that the material had a basic character,
255 and therefore, most functional groups had a basic character in their composition. Indeed, SO₂ is a
256 Lewis acid in which S is an acceptor atom that will strongly interact with basic surface materials to
257 form stable complexes (Rezaei et al., 2015). According to Shafeeyan et al. (2010), the basicity of
258 carbon materials are primary related to delocalized π -electrons of graphene layers that attract
259 protons as well as basic surface functionalities, i.e., nitrogen-containing groups or oxygen-
260 containing surface functionalities such as chromene, ketone, and pyrone. Fig. 4 b) shows that little
261 amount of nitrogen (0.2 %) is present in H2OBWB; thus, its basic character (pH = 8.6) does not
262 come from nitrogenated groups connected to their surface. Although KOHBBS had one of the
263 highest percentage of nitrogen (2.7 %), acid-oxygenated groups (16.2 %), surface area (1662 m² g⁻¹)
264 ¹), and micropore volume (0.72 cm³ g⁻¹), its SO₂ sorption capacity was one of the lowest (26.4 mg
265 g⁻¹). As mentioned earlier, this result can be explained by the incapability of SO₂ oxidation into
266 SO₃ inside micropores (Raymundo-Piñero et al., 2000).

267 The comparative SO₂ sorption capacity of carbon-derived materials in the available literature
268 is presented in Table 2. For most of materials listed, the porosity and surface area created after a
269 thermal treatment or activation (Atanes et al., 2012; Davini, 2001), and the presence of mineral
270 components and mostly nitrogen content, have created complexes with SO₂ (Xu et al., 2016) and a
271 basic character (Sun et al., 2016), respectively, which played a major role in their performance of

272 SO₂ adsorption. Also, the impregnation of nitrogenated groups on the surface of activated biochars
273 showed an enhancement of SO₂ adsorption (Shao et al., 2018). However, this procedure could be
274 an extra expenditure in industry during the production of activated carbons. An option that is
275 currently under study is the use of wood from construction waste that contains some amount of
276 resin or nitrogenated compounds that could improve the basicity of steam-activated biochar and
277 consequently the interactions with SO₂.

278 3.2 Activated biochar regeneration

279 Regeneration of activated biochars is an important asset necessary for industrial applications
280 so that sorbents can be reused in successive adsorption–desorption cycles (Braghiroli et al., 2018).
281 To investigate the regeneration and stability of activated biochars, six regeneration cycles were
282 performed. Materials were regenerated under thermal treatment at 600 °C for 1 h in an inert
283 atmosphere. Throughout the thermal regeneration of activated biochars after SO₂ adsorption, H₂SO₄
284 sorbed on the materials' structure is removed by the reduction of carbon, following the Eq.
285 7 (Knoblauch et al., 1981). These gas products (SO₂, CO₂, and H₂O) may also further react to
286 produce elemental sulfur, SO₂ or H₂SO₄ (Knoblauch et al., 1981; Richter, 1990). According to Cui
287 et al. (2018), the higher temperature (from 400 to 600 °C), the better desulfurization activity of
288 coke materials after regeneration. At 600 °C, the interactions established between the adsorbate and
289 adsorbent are able to break.



291 The regeneration efficiency of H2OBWB was evaluated due to its better performance for SO₂
292 uptake comparing to the other activated biochars. SO₂ breakthrough curves and SO₂ adsorption
293 capacity of H2OBWB before and after six adsorption–desorption cycles are illustrated in Fig. 5 a)
294 and b), respectively. As can be seen in Fig. 5, after each cycle, the SO₂ removal capacity of
295 H2OBWB decreases (approx. 60 mg g⁻¹) compared to cycle 0 (76.9 mg g⁻¹), but it then increases to

296 up 85.3 mg g⁻¹ (cycle 5). PSD curves of H2OBWB and H2OBWB after four, five and six
297 adsorption-desorption cycle experiments are presented in Fig. 6. It is clearly seen that the pore
298 structure of activated biochar was altered after these regeneration cycles, which led to a slight
299 increase in its surface area and micropore volume with a reduction of mesopores that in turn favored
300 the storage capacity of H₂SO₄ and therefore the SO₂ adsorption capacity. Indeed, the surface area
301 and micropore volume have increased to approximately 680 m² g⁻¹ and 0.26 cm³ g⁻¹, respectively
302 (cycle 6), compared to 590 m² g⁻¹ and 0.23 cm³ g⁻¹ (cycle 0). After SO₂ adsorption test, the acid
303 surface (pH = 3.2) of H2OBWB increased but then decomposed at 600 °C during the SO₂
304 desorption test, leaving a new basic surface (pH = 8.3) that favored SO₂ sorption capacity.
305 Consequently, it is possible that the surface chemistry of the regenerated material is more suitable
306 for SO₂ adsorption than that of the original H2OBWB.

307 4. Conclusion

308 The capacity of activated biochars to enhance adsorption of SO₂ was investigated according to
309 materials' porous structure and surface chemistry. No linear relationship was observed between
310 surface area; total, micropore, mesopore, and ultramicropore volume of activated biochars; and SO₂
311 sorbed from dynamic adsorption tests. KOH-activated biochars, the most porous materials (up to
312 1700 m² g⁻¹) with a wide microporosity, had less uptake of SO₂ once their capacity for SO₂
313 oxidation into SO₃ did not occur. Nitrogen-basic groups of up to 2.5 % were not enough to improve
314 the performance of KOH-activated biochars for SO₂ sorption. On the other hand, steam-activated
315 biochar had an optimal moderate surface area (590 m² g⁻¹) and porous structure, a basic character,
316 and a low proportion of acid-oxygenated functional groups connected to its surface, which played
317 an important role on its performance for SO₂ adsorption. After the thermal regeneration of activated
318 biochar, results suggested that H2OBWB had high SO₂ removal capacity and suitability for

319 successive adsorption–desorption cycles. Therefore, activated biochar made from forest wood
320 residues in the presence of steam at 900 °C is a promising potential adsorbent material for the
321 efficient removal of SO₂ contaminant.

322 **Acknowledgments**

323 This research was funded by the Québec’s Ministry of Economy, Science and Innovation (Ministère
324 de l’Économie, de la Science et de l’Innovation du Québec), the Natural Sciences and Engineering
325 Research Council of Canada (NSERC), the Canada Research Chair Program, the College of
326 Abitibi-Témiscamingue, and the Technology Centre for Industrial Waste (Centre Technologique
327 des Résidus Industriels) through its partner on this project, Airex Energy. The first author, Dr.
328 Flavia Lega Braghiroli, also sincerely acknowledges NSERC financial support via a Banting
329 Postdoctoral Fellowship (2017–2019). The authors also thank Gilles Villeneuve and Hélié Jacob
330 Turmel for their assistance with experiments, analysis, and testing in the laboratory.

331

332 **References**

- 333 Abdurashed, A.A., Jalil, A.A., Triwahyono, S., Zaini, M.A.A., Gambo, Y., Ibrahim, M., 2018.
334 Surface modification of activated carbon for adsorption of SO₂ and NO_x: a review of
335 existing and emerging technologies. *Renew. Sustain. Energy Rev.* 94, 1067–1085.
336 <https://doi.org/10.1016/j.rser.2018.07.011>
- 337 ASTM Standard D6646-03, 2008. Test method for determination of the accelerated hydrogen
338 sulfide breakthrough capacity of granular and pelletized activated carbon. ASTM
339 International, West Conshohocken. <https://doi.org/10.1520/D6646-03R14>
- 340 Atanes, E., Nieto-Márquez, A., Cambra, A., Ruiz-Pérez, M.C., Fernández-Martínez, F., 2012.
341 Adsorption of SO₂ onto waste cork powder-derived activated carbons. *Chem. Eng. J.* 211–
342 212, 60–67. <https://doi.org/10.1016/j.cej.2012.09.043>
- 343 Bagreev, A., Bashkova, S., Bandosz, T.J., 2002. Adsorption of SO₂ on activated carbons: the
344 effect of nitrogen functionality and pore sizes. *Langmuir* 18, 1257–1264.
345 <https://doi.org/10.1021/la011320e>
- 346 Bamdad, H., Hawboldt, K., MacQuarrie, S., 2018. A review on common adsorbents for acid gases
347 removal: focus on biochar. *Renew. Sustain. Energy Rev.* 81, 1705–1720.
348 <https://doi.org/10.1016/j.rser.2017.05.261>
- 349 Braghiroli, F.L., Bouafif, H., Hamza, N., Neculita, C.M., Koubaa, A., 2018. Production,
350 characterization, and potential of activated biochar as adsorbent for phenolic compounds
351 from leachates in a lumber industry site. *Environ. Sci. Pollut. Res.* 25, 26562–26575.
352 <https://doi.org/10.1007/s11356-018-2712-9>
- 353 Brunauer, S., Emmett, P.H., Teller, E., 1938. Adsorption of gases in multimolecular layers. *J.*
354 *Am. Chem. Soc.* 60, 309–319. <https://doi.org/10.1021/ja01269a023>
- 355 Cui, X., Yi, H., Tang, X., Zhao, S., Yang, K., Yan, B., Li, C., Yang, X., Feng, T., Ma, Y., 2018.
356 Study of the properties of adsorption of SO₂- thermal regeneration cycle of activated coke
357 modified by oxidization: study of the properties of adsorption of SO₂. *J. Chem. Technol.*
358 *Biotechnol.* 93, 720–729. <https://doi.org/10.1002/jctb.5421>
- 359 Davini, P., 2001. SO₂ adsorption by activated carbons with various burnoffs obtained from a
360 bituminous coal. *Carbon* 39, 1387–1393. [https://doi.org/10.1016/S0008-6223\(00\)00258-X](https://doi.org/10.1016/S0008-6223(00)00258-X)
- 361 Dehkhoda, A.M., Gyenge, E., Ellis, N., 2016. A novel method to tailor the porous structure of
362 KOH-activated biochar and its application in capacitive deionization and energy storage.
363 *Biomass Bioenergy* 87, 107–121. <https://doi.org/10.1016/j.biombioe.2016.02.023>
- 364 Dubinin, M.M., 1989. Fundamentals of the theory of adsorption in micropores of carbon
365 adsorbents: Characteristics of their adsorption properties and microporous structures.
366 *Carbon* 27, 457–467. [https://doi.org/10.1016/0008-6223\(89\)90078-X](https://doi.org/10.1016/0008-6223(89)90078-X)
- 367 Environment and Climate Change Canada, 2018. Canada-United States Air Quality Agreement
368 Progress Report 2012. Available at [https://www.canada.ca/en/environment-climate-
369 change/services/air-pollution/publications/canada-united-states-air-quality-report-
370 2012/introduction.html](https://www.canada.ca/en/environment-climate-change/services/air-pollution/publications/canada-united-states-air-quality-report-2012/introduction.html) (accessed 8.14.18).
- 371 Fioletov, V.E., McLinden, C.A., Krotkov, N., Li, C., Joiner, J., Theys, N., Carn, S., Moran, M.D.,
372 2016. A global catalogue of large SO₂ sources and emissions derived from the Ozone
373 Monitoring Instrument. *Atmospheric Chem. Phys.* 16, 11497–11519.
374 <https://doi.org/10.5194/acp-16-11497-2016>
- 375 Gargiulo, V., Gomis-Berenguer, A., Giudicianni, P., Ania, C.O., Ragucci, R., Alfè, M., 2018.
376 Assessing the potential of biochars prepared by steam-assisted slow pyrolysis for CO₂

377 adsorption and separation. *Energy Fuels* 32, 10218–10227.
378 <https://doi.org/10.1021/acs.energyfuels.8b01058>

379 Giudicianni, P., Pindozzi, S., Grottola, C.M., Stanzione, F., Faugno, S., Fagnano, M., Fiorentino,
380 N., Ragucci, R., 2017. Pyrolysis for exploitation of biomasses selected for soil
381 phytoremediation: characterization of gaseous and solid products. *Waste Manag.* 61, 288–
382 299. <https://doi.org/10.1016/j.wasman.2017.01.031>

383 Gregg, S.J., Sing, K.S.W., 1991. Adsorption, surface area, and porosity. Academic Press' london,
384 UK.

385 He, B., Zheng, X., Wen, Y., Tong, H., Chen, M., Chen, C., 2003. Temperature impact on SO₂
386 removal efficiency by ammonia gas scrubbing. *Energy Convers. Manag.* 44, 2175–2188.
387 [https://doi.org/10.1016/S0196-8904\(02\)00230-3](https://doi.org/10.1016/S0196-8904(02)00230-3)

388 Izquierdo, M.T., Rubio, B., Mayoral, C., Andrés, J.M., 2003. Low cost coal-based carbons for
389 combined SO₂ and NO removal from exhaust gas. *Fuel* 82, 147–151.
390 [https://doi.org/10.1016/S0016-2361\(02\)00249-1](https://doi.org/10.1016/S0016-2361(02)00249-1)

391 Karatepe, N., Orbak, İ., Yavuz, R., Özyuğuran, A., 2008. Sulfur dioxide adsorption by activated
392 carbons having different textural and chemical properties. *Fuel* 87, 3207–3215.
393 <https://doi.org/10.1016/j.fuel.2008.06.002>

394 Khaniabadi, Y.O., Daryanoosh, S.M., Hopke, P.K., Ferrante, M., De Marco, A., Sicard, P.,
395 Oliveri Conti, G., Goudarzi, G., Basiri, H., Mohammadi, M.J., Keishams, F., 2017. Acute
396 myocardial infarction and COPD attributed to ambient SO₂ in Iran. *Environ. Res.* 156,
397 683–687. <https://doi.org/10.1016/j.envres.2017.04.028>

398 Knoblauch, K., Richter, E., Jüntgen, H., 1981. Application of active coke in processes of SO₂-
399 and NO_x-removal from flue gases. *Fuel* 60, 832–838. [https://doi.org/10.1016/0016-2361\(81\)90146-0](https://doi.org/10.1016/0016-2361(81)90146-0)

400

401 Li, K., Ling, L., Lu, C., Qiao, W., Liu, Z., Liu, L., Mochida, I., 2001. Catalytic removal of SO₂
402 over ammonia-activated carbon fibers. *Carbon* 39, 1803–1808.
403 [https://doi.org/10.1016/S0008-6223\(00\)00320-1](https://doi.org/10.1016/S0008-6223(00)00320-1)

404 Li, X., Zhu, C., 2016. Gas-liquid mass transfer with instantaneous chemical reaction in a slurry
405 bubble column containing fine reactant particles. *Chem. Ind. Chem. Eng. Q.* 22, 85–93.
406 <https://doi.org/10.2298/CICEQ141001021L>

407 Lisovskii, A., Semiat, R., Aharoni, C., 1997. Adsorption of sulfur dioxide by active carbon treated
408 by nitric acid: I. Effect of the treatment on adsorption of SO₂ and extractability of the acid
409 formed. *Carbon* 35, 1639–1643. [https://doi.org/10.1016/S0008-6223\(97\)00129-2](https://doi.org/10.1016/S0008-6223(97)00129-2)

410 Lua, A.C., Guo, J., 2000. Activated carbon prepared from oil palm stone by one-step CO₂
411 activation for gaseous pollutant removal. *Carbon* 38, 1089–1097.
412 [https://doi.org/10.1016/S0008-6223\(99\)00231-6](https://doi.org/10.1016/S0008-6223(99)00231-6)

413 Marsh, H., Rodríguez-Reinoso, F., 2006. Activated carbon, 1st ed. Elsevier, Amsterdam, NL.

414 Mohamad Nor, N., Lau, L.C., Lee, K.T., Mohamed, A.R., 2013. Synthesis of activated carbon
415 from lignocellulosic biomass and its applications in air pollution control—a review. *J.*
416 *Environ. Chem. Eng.* 1, 658–666. <https://doi.org/10.1016/j.jece.2013.09.017>

417 Rangabhashiyam, S., Balasubramanian, P., 2019. The potential of lignocellulosic biomass
418 precursors for biochar production: performance, mechanism and wastewater application—
419 a review. *Ind. Crops Prod.* 128, 405–423. <https://doi.org/10.1016/j.indcrop.2018.11.041>

420 Raymundo-Piñero, E., Cazorla-Amorós, D., Salinas-Martínez de Lecea, C., Linares-Solano, A.,
421 2000. Factors controlling the SO₂ removal by porous carbons: relevance of the SO₂
422 oxidation step. *Carbon* 38, 335–344. [https://doi.org/10.1016/S0008-6223\(99\)00109-8](https://doi.org/10.1016/S0008-6223(99)00109-8)

423 Rezaei, F., Rownaghi, A.A., Monjezi, S., Lively, R.P., Jones, C.W., 2015. SO_x/NO_x removal from
424 flue gas streams by solid adsorbents: a review of current challenges and future directions.
425 Energy Fuels 29, 5467–5486. <https://doi.org/10.1021/acs.energyfuels.5b01286>
426 Richter, E., 1990. Carbon catalysts for pollution control. Catal. Today 7, 93–112.
427 [https://doi.org/10.1016/0920-5861\(90\)85011-C](https://doi.org/10.1016/0920-5861(90)85011-C)
428 Shafeeyan, M.S., Daud, W.M.A.W., Houshmand, A., Shamiri, A., 2010. A review on surface
429 modification of activated carbon for carbon dioxide adsorption. J. Anal. Appl. Pyrolysis
430 89, 143–151. <https://doi.org/10.1016/j.jaap.2010.07.006>
431 Shao, J., Zhang, J., Zhang, X., Feng, Y., Zhang, H., Zhang, S., Chen, H., 2018. Enhance SO₂
432 adsorption performance of biochar modified by CO₂ activation and amine impregnation.
433 Fuel 224, 138–146. <https://doi.org/10.1016/j.fuel.2018.03.064>
434 Sing, K.S.W., 1985. Reporting physisorption data for gas/solid systems with special reference to
435 the determination of surface area and porosity (Recommendations 1984). Pure Appl.
436 Chem. 57, 603–619. <https://doi.org/10.1351/pac198557040603>
437 Slack, A.V., Falkenberry, H.L., Harrington, R.E., 1972. Sulfur oxide removal from waste gases:
438 lime-limestone scrubbing technology. J. Air Pollut. Control Assoc. 22, 159–166.
439 <https://doi.org/10.1080/00022470.1972.10469622>
440 Stoeckli, F., Ballerini, L., 1991. Evolution of microporosity during activation of carbon. Fuel 70,
441 557–559. [https://doi.org/10.1016/0016-2361\(91\)90036-A](https://doi.org/10.1016/0016-2361(91)90036-A)
442 Sun, F., Gao, J., Liu, X., Yang, Y., Wu, S., 2016. Controllable nitrogen introduction into porous
443 carbon with porosity retaining for investigating nitrogen doping effect on SO₂ adsorption.
444 Chem. Eng. J. 290, 116–124. <https://doi.org/10.1016/j.cej.2015.12.044>
445 Sun, F., Gao, J., Zhu, Y., Chen, G., Wu, S., Qin, Y., 2013. Adsorption of SO₂ by typical
446 carbonaceous material: a comparative study of carbon nanotubes and activated carbons.
447 Adsorption 19, 959–966. <https://doi.org/10.1007/s10450-013-9504-9>
448 Sun, F., Gao, J., Zhu, Y., Qin, Y., 2011. Mechanism of SO₂ adsorption and desorption on
449 commercial activated coke. Korean J. Chem. Eng. 28, 2218–2225.
450 <https://doi.org/10.1007/s11814-011-0078-5>
451 Tarazona, P., 1995. Solid-fluid transition and interfaces with density functional approaches. Proc.
452 14th Eur. Conf. Surf. Sci. 331, 989–994. [https://doi.org/10.1016/0039-6028\(95\)00170-0](https://doi.org/10.1016/0039-6028(95)00170-0)
453 UNECE, 2018. The 1994 Oslo Protocol on Further Reduction of Sulphur Emissions. Available at:
454 https://www.unece.org/env/lrtap/fsulf_h1.html (accessed 8.14.18).
455 Xu, X., Huang, D., Zhao, L., Kan, Y., Cao, X., 2016. Role of inherent inorganic constituents in
456 SO₂ sorption ability of biochars derived from three biomass wastes. Environ. Sci. Technol.
457 50, 12957–12965. <https://doi.org/10.1021/acs.est.6b03077>
458 Zhu, Y., Gao, Jihui, Li, Y., Sun, F., Gao, Jianmin, Wu, S., Qin, Y., 2012. Preparation of activated
459 carbons for SO₂ adsorption by CO₂ and steam activation. J. Taiwan Inst. Chem. Eng. 43,
460 112–119. <https://doi.org/10.1016/j.jtice.2011.06.009>
461
462
463

464 **Captions of tables**

465 **Fig. 1.** SO₂ removal efficiency curves as function of saturation adsorption time for a) BWB- and b)
466 BBS-activated materials.

467 **Fig. 2.** a) and b) N₂ adsorption–desorption isotherms (full and open symbols, respectively) at -196
468 °C; c) and d) PSD determined by the DFT method and N₂ isotherms; e) and f) CO₂
469 adsorption isotherms at 0 °C; g) and h) PSD determined by the DFT method and CO₂
470 isotherms for activated biochars made from birch and spruce, respectively.

471 **Fig. 3.** Relationship between SO₂ uptake and a) surface area, b) micropore volume, c)
472 mesopore volume, d) ultramicropore volume and e) average micropore width of
473 biochars (●) and KOH (◆), CO₂ (■), and steam-activated biochars (▲).

474 **Fig. 4.** Relationship between SO₂ uptake and a) percentage of acid-oxygenated groups measured
475 by XPS and b) percentage of nitrogen measured by elemental analysis of biochars (●) and
476 KOH (◆), CO₂ (■) and steam-activated biochars (▲).

477 **Fig. 5.** a) SO₂ concentration adsorbed as function of breakthrough time, and b) SO₂ adsorption
478 capacity of H2OBWB after six adsorption–desorption cycles.

479 **Fig. 6.** PSD determined by the DFT method and N₂ isotherms for H2OBWB and H2OBWB after
480 four, five and six adsorption-desorption cycle experiments.

481

482

483

484

485

486

487 **Captions of figures**

488 **Table 1.** pH, saturation adsorption time, SO₂ saturation capacities, and contributions to the C1s
489 bands in XPS patterns for biochar-derived materials

490 **Table 2:** Comparative SO₂ sorption capacity of carbon-derived materials

491
492
493
494
495
496
497
498
499
500
501
502
503
504
505
506
507
508
509
510
511
512
513
514
515
516
517
518
519
520
521
522
523
524
525
526
527

528 **Table 1.** pH, saturation adsorption time, SO₂ saturation capacities, and contributions to the C1s
 529 bands in XPS patterns for biochar-derived materials

	BWB	BBS	KOHBWB	KOHBBS	CO2BWB	CO2BBS	H2OBWB	H2OBBS
pH _i	5.9	7.1	9.9	10.2	9.5	10.0	8.6	9.7
pH _f	4.1	4.4	2.5	2.5	2.1	2.9	3.3	3.2
Breakthrough time (min)	21.3	21.2	36.5	27.1	58.3	26.1	78.5	27.5
SO ₂ capacity (mg g ⁻¹)	20.4	20.3	35.3	26.4	56.9	25.0	76.9	26.5
XPS analysis	Binding energy (BE) (eV) and area of the peak (%)							
BE < 285eV (graphitic sp ² carbon)	68.0	72.0	61.8	65.4	72.1	75.8	67.6	72.8
285.7 < BE < 287.1 (C-OH)	17.1	18.4	14.7	8.1	12.8	11.7	8.1	4.1
286.1 < BE < 288 (C=O or O-C-O)	4.6	3.5	7.3	7.9	4.5	3.4	6.9	6.4
288 < BE < 289.4 (O=C-O)	4.6	2.2	3.4	6.4	2.2	2.4	2.9	2.9
Total oxygenated groups	26.3	24.1	25.4	22.4	19.5	17.5	17.9	13.4
BE > 290 ("Shake-up" satellites)	5.7	3.9	12.8	12.2	8.4	6.7	14.5	13.8

530

531
 532
 533
 534
 535
 536
 537
 538
 539
 540
 541
 542
 543
 544
 545
 546
 547

548 **Table 2:** Comparative SO₂ sorption capacity of carbon-derived material

Material precursor	Materials treatment	Experimental conditions	S _{BET} (m ² g ⁻¹)	SO ₂ adsorption capacity (mg g ⁻¹)	N (wt.%)	References
Biochar made from dairy manure (DM), sewage sludge (SS), and rice husk (RH)	Pyrolysis at 500 °C	Dynamic tests; Room temperature; Glass column: 25 cm length, 5 cm diameter, 2.5 cm length of sample (3.8–8 g); 0.5% SO ₂ (5000 ppm) with ambient air; Flow rate: 1.5 L min ⁻¹	DM: 4.8 SS: 10 RH: 41	DM: 64 SS: 35 RH: 13	DM: 2.2 SS: 3.3 RH: 0.6	(Xu et al., 2016)
Carbon fibers made from ethylene tar	Activation in presence of steam (S) and ammonia (N) at 800–915 °C	Fixed-bed reactor; 30 °C; SO ₂ (2000 ppm) with or without 5% vol. O ₂ ; Total flow rate: 100 mL min ⁻¹	S: 1469 N: 1480	S: 11 N: 28	S: 0.01 N: 1.1	(Li et al., 2001)
N-doped carbon made from polymerization of phenol, melamine, and formaldehyde	Pyrolysis at 900 °C	Fixed-bed reactor; 25 °C; 0.1 g sample; SO ₂ (500 ppm), N ₂ balance; Total flow rate: 200 mL min ⁻¹	1013	48	10 (at.%)	(Sun et al., 2016)
Activated pyrolysed bituminous coal	Pyrolysis at 700 °C and further activation in presence of CO ₂ at 900 °C	Thermogravimetric analyser; 100 °C; SO ₂ (1000 ppm), O ₂ (3%), CO ₂ (10%), water vapour (10%) in N ₂	740	92	-	(Davini, 2001)
Activated biochar made from cork powder	Pyrolysis at 750 °C and further activation in presence of KOH or CO ₂ at 750 °C	Thermogravimetric analyser; 45 °C; SO ₂ (500–10000 ppm), N ₂ balance; Total flow rate: 120 mL min ⁻¹	KOH: 584 CO ₂ : 76	KOH: 90 CO ₂ : 65	KOH: 0.3 CO ₂ : 1.5	(Atanes et al., 2012)
Activated biochar made from corncobs	Pyrolysis at 600 °C followed by activation in presence of CO ₂ at 850 °C and further impregnation with methyldiethanolamine	Fixed-bed reactor; 120 °C; 1% SO ₂ (20 mL min ⁻¹) and N ₂ (80 mL min ⁻¹)	-	156	6.5 (at.%)	(Shao et al., 2018)
Commercial coconut shell activated carbon	-	Fixed-bed reactor; 150–200 °C; 1 g sample; SO ₂ (1000 ppm), N ₂ balance; Total flow rate: 1 L min ⁻¹	748	21	-	(Sun et al., 2013)
Commercial single wall carbon nanotube	-	Fixed-bed reactor; 150–200 °C; 1 g sample; SO ₂ (1000 ppm); N ₂ balance; Total flow rate: 1 L min ⁻¹	404	4	-	(Sun et al., 2013)
Commercial activated carbon (Panreac)	-	Thermogravimetric analyser; 45 °C; SO ₂ (500–10000 ppm), N ₂ balance; Total flow rate: 120 mL min ⁻¹	752	65	0.2	(Atanes et al., 2012)
Commercial activated coke	-	Fixed-bed reactor; 5 g sample	563	53	0.6	(Sun et al., 2011)

Activated biochar made from wood residues	Pyrolysis at 454 °C and further activation in presence of steam at 900 °C	Dynamic tests; Room temperature; Glass column: 27 cm length; 2.5 cm diameter; 23 cm length of sample (10–25 g); SO ₂ (50 ppm) with moist air; Flow rate: 30 mL min ⁻¹ ;	590	77	0.2	This work
---	---	---	-----	----	-----	------------------

549